Nanoparticle-Fluid Interactions at Ultra-High Acoustic

Vibration Frequencies Studied by Femtosecond Time-Resolved

Microscopy

Kuai Yu<sup>1\*</sup>, Yang Yang<sup>1</sup>, Junzhong Wang<sup>1</sup>, Gregory V. Hartland<sup>2\*</sup>, Guo Ping Wang<sup>1\*</sup>

<sup>&</sup>lt;sup>1</sup> Institute of Microscale Optoelectronics, Shenzhen University, Shenzhen 518060, China

<sup>&</sup>lt;sup>2</sup> Department of Chemistry and Biochemistry, University of Notre Dame, Notre Dame, Indiana 46556, United States

## **ABSTRACT:**

Liquid viscous and viscoelastic properties are very important parameters in determining rheological phenomena. Mechanical resonators with extremely high vibrational frequencies interacting with simple liquids present a wide range of applications from mass sensing to biomechanics. However, a lack of understanding of fluid viscoelasticity greatly hinders the utilization of mechanical resonators. In this paper the high frequency acoustic vibrations of Au nanoplates with large quality factors were used to probe fluid properties (water, glycerol and their mixtures) through time-resolved pump-probe microscopy experiments. For water viscous damping was clearly observed, where an inviscid effect was only detected previously. Adding glycerol to the water increases the fluid viscosity, and leads to a bulk viscoelastic response in the system. The experimental results are in excellent agreement with a continuum mechanics model for the damping of nanoplate breathing modes in liquids, confirming the experimental observation of viscoelastic effects. In addition to the breathing modes of the nanoplates, Brillouin oscillations are observed in the experiments. Analysis of the frequency of the Brillouin oscillations also shows the presence of viscoelastic effects in the high viscosity solvents. The detection and analysis of viscous damping in liquids is important not just for understanding the energy dissipation mechanisms and providing the mechanical relaxation times in the liquids, but also for developing applications of nanomechanical resonators for fluid environments.

KEYWORDS: acoustic vibration, fluid mechanics, fluid viscoelasticity, molecular relaxation time, nanoplate, transient absorption microscopy

# **INTRODUCTION**

Nanoparticle-fluid interactions represent an active area of research and has attracted broad attention especially for nanoparticle mechanical vibrations at ultra-high frequencies (GHz to THz range), where the vibrational periods can be comparable to the liquid relaxation times. Understanding how vibrational energy dissipation depends on the fluid properties is prerequisite for designing high quality-factor mechanical resonators that can operate in liquids. Pecently, simple liquids interacting with high frequency resonators have shown the emergence of viscoelastic effects. The strength of this effect depends on the form of the vibrational mode and the Deborah number for the liquid:  $De = \omega \lambda$ , where  $\omega$  is the frequency of the vibration and  $\lambda$  is the relaxation time of the liquid. Calculations and experimental results show that significant viscoelastic effects occur for vibrational modes that generate shear. However, for breathing modes, which create compressional motions in the liquids, effects from viscoelasticity are often (usually) masked by the inviscid response of the liquid. Pecanterial results and the properties of the liquid.

A straightforward way to facilitate the observation of fluid viscoelasticity in these experiments is to increase the vibration frequency by reducing the nanostructure size (higher frequencies produce larger Deborah numbers for a given liquid). A variety of techniques have been used to study the mechanical vibrations of metal nanoparticles. <sup>2, 8, 21, 22</sup> The most sensitive of these, and therefore the most appropriate for studies of small particles, are transient absorption spectroscopy and Raman spectroscopy. <sup>23</sup> These techniques have been used to study particles with dimensions on the order of a few nm, and corresponding acoustic mode frequencies of several THz. <sup>23, 24</sup> However, for accurate measurements of the fluid damping mechanism high quality factors are also needed. <sup>14, 15, 20</sup> This can only be achieved by studying single particles, which is a challenge for nm size particles. Recently two dimensional gold nanoplates (NPLs) were shown to

have breathing mode vibrations with large quality factors in the frequency range of ~100 GHz.<sup>25-27</sup> Thus, this system is an excellent choice for interrogating fluid-nanoparticle interactions – if the NPLs can be made thin enough to support ultra-high frequency vibrations.

In this study, we optimized the synthesis of the Au NPLs to produce thicknesses of ~10 nm and concomitant breathing mode frequencies of up to ~160 GHz, while still maintaining large vibration quality factors. High quality factors were achieved by suspending the NPLs over pores in a substrate. This is possible due to the large in-plane sizes of the NPLs. The damping of the breathing modes of single Au NPLs in simple liquids (water-glycerol mixtures) were examined by time-resolved pump-probe microscopy experiments. By measuring the lifetimes in air and the liquid, the contribution from the liquid to the damping was determined. The average quality factors for fluid damping were found to be significantly smaller than the values expected for simple radiation of sound waves into the fluid, indicating the presence of viscous and/or viscoelastic effects in the fluid. Brillouin oscillations were also observed for NPLs in the fluid environments. This effect arises from interference between reflected probe light from the NPLs and acoustic waves generated in the liquid. <sup>28-31</sup> For high viscosity fluids the speed of sound derived from the Brillouin oscillation frequency is significantly different to the literature value. <sup>32-34</sup>

In order to understand the experimental results, a continuum mechanics model was developed to calculate the frequencies and lifetimes of the NPL breathing modes in liquid environments. The calculations show that viscous effects are important for water, which is surprising given its low viscosity. On the other hand, as the viscosity of the liquid is increased by adding glycerol, viscoelastic effects become dominant. Viscoelastic effects are included in the calculations by scaling the solvent viscosities by a factor  $(1 - i\omega\lambda)^{-1}$ , where  $\lambda$  is the relaxation time in the fluid. We show that this simple relation also explains the difference between the

measured and expected Brillouin oscillation frequencies. As a whole, this paper demonstrates that transient absorption microscopy measurements of metal nanostructures is a powerful way to interrogate the properties of liquids.

## **RESULTS AND DISCUSSION**

High-quality mechanical resonators with high vibrational frequencies are desirable for many studies, from fundamental research to mass sensing applications.  $^{27, 35, 36}$  One of the difficulties is reliably producing this type of mechanical resonator with high quality factors and large interaction areas. Two-dimensional Au NPLs are an excellent candidate, as they have large in-plane areas with size >100  $\mu$ m² and vibrational frequencies >100 GHz. However, chemically synthesizing thin Au NPLs with thickness of ~10 nm and edge length/thickness aspect ratio >1000 is difficult to achieve. Although Au NPLs with thicknesses of ~10 nm were previously reported, they were either formed on substrates, not uniform across the whole NPL, or had small in-plane areas with an aspect ratio <100.  $^{37-39}$ 

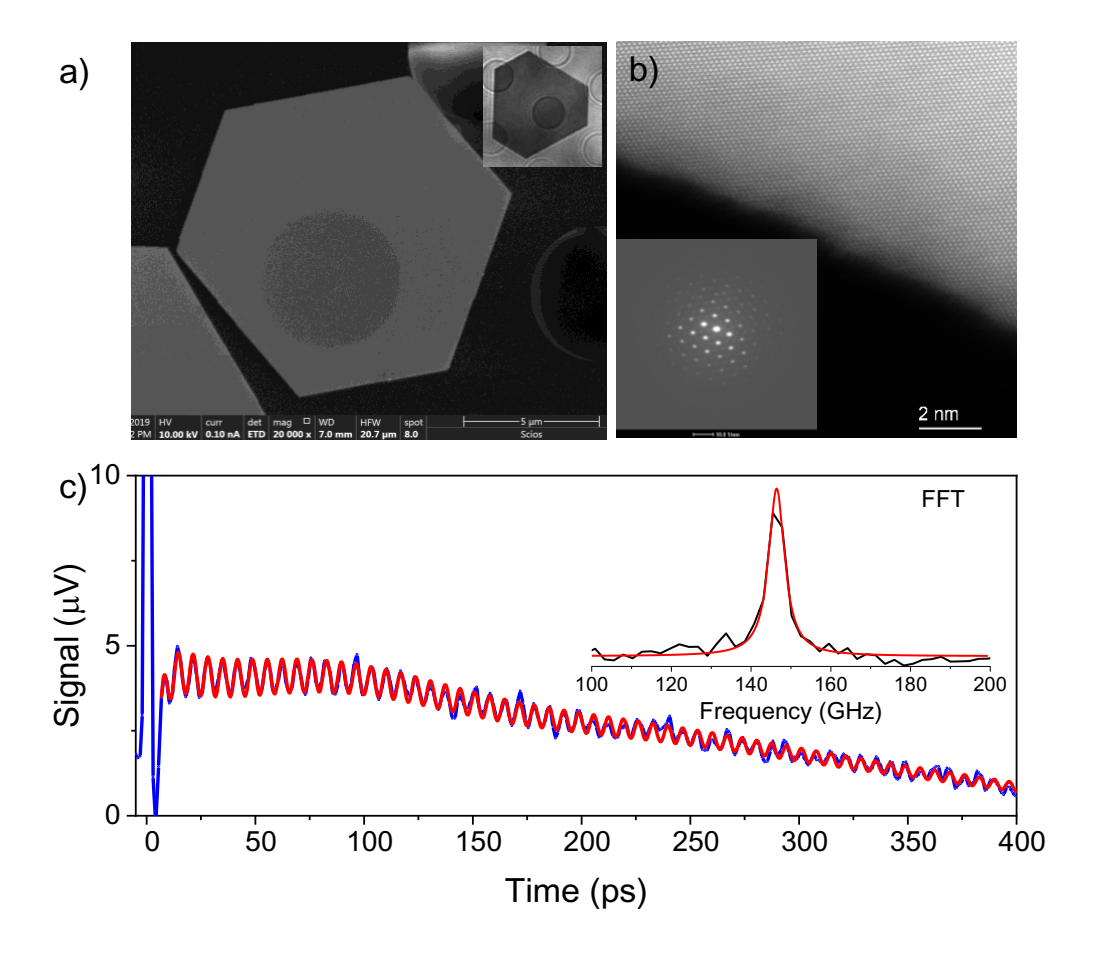


Figure 1. (a) SEM image of a Au NPL suspended over a pore of a holey silicon nitride film. The inset shows an optical image of a single Au NPL. The underlying hole structures are clearly observable in both electron microscopy and optical images indicating the thin plate thickness. (b) High-resolution TEM image of a Au NPL and the corresponding SAED pattern which showing the high-quality single-crystalline nature of the Au NPLs with {111} surfaces planes. (c) Transient absorption trace of a single suspended Au NPL in air. The red line shows a fit to the data using the damped cosine function. Inset: the corresponding FFT spectrum of the oscillatory signal with a Lorentz curve fitting in red. The vibrational frequency and quality factor are  $f_{air} = 146.6 \pm 0.09$  GHz and  $Q_{air} = 118 \pm 12$ , respectively.

We synthesized Au NPLs following a previous procedure with slight modifications (see Experimental methods for more details).40, 41 A combination of binary surfactants of Poly(vinylpyrrolidone) (PVP) and cetyltrimethylammonium bromide (CTAB) were used. The PVP acted as both reducing agent and surfactant and was found to preferentially adsorb on the edge of Au NPLs to promote the in-plane growth, while the CTAB is adsorbed on the basal facets to stabilize the nanocrystals. 42 Note that the addition of CTAB at the right amount is critical for the formation of thin Au NPLs. Without the addition of CTAB, Au NPLs with thickness of tens of nanometers are normally synthesized. Figure 1(a) shows a scanning electron microscopy (SEM) image of Au NPLs supported on holey silicon nitride films. The underlying pore structure is clearly visible for both the electron and optical microscopy images (shown in the inset of Figure 1(a)), which facilitate the study of the vibrations of the suspended NPLs without perturbations of the substrate. Figure S1 gives a wider view of the Au NPL sample. The NPLs are mostly hexagonal shapes with edge lengths of 10-20 µm. Figure 1(b) shows a high-resolution transmission electron microscopy (TEM) image of a Au NPL and the corresponding selected area electron diffraction (SAED) pattern (inset). The images and diffraction pattern are consistent with the face-centered cubic (fcc) structure of gold, with the NPL surface corresponding to the {111} basal planes. There are no obvious polymer surfactants left on the surfaces as seen from the edge of the high-resolution TEM image.

A representative transient absorption trace of a suspended Au NPL in air is shown in Figure 1(c). The pump-probe signal shows an initial fast decay, that corresponds to the rapid cooling of the excited electrons through electron-phonon coupling.<sup>7</sup> The slower oscillating signal after several picoseconds delay is due to the breathing mode vibrations in the thickness direction of the Au NPL. These vibrations are impulsively excited by the fast laser-induced heating of the crystal lattice.<sup>43</sup>

Since the lateral dimensions of the Au NPLs are much larger than their thickness and the laser excitation spot ( $\sim 1 \mu m$ ), only the breathing vibration corresponding to changes in the thickness is detected.<sup>37</sup> The vibrational parameters are obtained by fitting the experimental data with the function:

$$\Delta I(t) = \sum_{K=(el,ph)} A_K \exp\left(-\frac{t}{\tau_K}\right) + \sum_{N=(1,2)} A_N \cos\left(\frac{2\pi t}{T_N} - \phi_N\right) \exp\left(-\frac{t}{\tau_N}\right)$$
(1)

where the first term accounts for the background signal due to cooling of the Au NPL from electron-phonon (K = el) and phonon-phonon (K = ph) interactions, and the second term accounts for vibrations. Two modes (N = 1,2) are included to describe the breathing mode and the Brillouin oscillations, and  $T_N$  and  $\tau_N$  are the vibrational period and damping time, respectively.

To compare the damping for different NPLs, the lifetimes are expressed in terms of quality factors  $Q_n = \pi \tau_N/T_N$ . This removes the trivial size dependence that arises from the way the lifetimes and periods scale with size.<sup>44, 45</sup> For the NPL in Figure 1 the vibrational frequency and quality factor are  $f_{air} = 146.6 \pm 0.09$  GHz and  $Q_{air} = 118 \pm 12$ , respectively. The errors are fitting uncertainties with 95% confidence limits which are on the order of 0.06% for the frequency and 10% for the lifetimes. The vibrational frequency corresponds to a thickness  $h \sim 11.7$  nm or  $\sim 48$  atomic layers for a free Au NPLs calculated by  $h = c_l/2f$  (the longitudinal speed of sound along the <111> direction of bulk gold of  $c_l = 3440$  m/s was used). This vibrational mode has been observed in previous investigations.<sup>37</sup> The obtained fitting parameters are also consistent with the fast Fourier transform (FFT) spectrum as shown in the inset of Figure 1(c). The high quality factors for these nanostructures are important for accurate measurements of liquid damping.

The oscillatory signals in Figure 1(c) can be well fitted by the damped cosine function and the fitting error for the frequency is extremely small (0.06%) due to the long vibrational lifetime.

However, the measurement accuracy for the vibrational frequency for a single Au NPL is also affected by system errors, which include the stability of the microscope and surface polymer coating inhomogeneity. Figure S2 shows the system errors from measuring a single Au NPL multiple times at different locations. The average frequency for the NPL in air is  $f_{air} = 111.43 \pm 0.15$  GHz, where the error represents the standard deviation. This indicates the aggregated measurement error is  $\sim 0.13\%$ . This level of accuracy for the vibrational frequency is sufficient to differentiate a single atomic layer thickness difference, and the sensitivity is comparable to the two-photon photoluminescence spectroscopy.<sup>38</sup> The narrow range of frequency values for the single Au NPL also indicates that the NPLs have smooth surfaces without terraces.

Since the suspended Au NPLs are away from the substrates (Figure 1) with negligible vibrational energy leakage, the measured quality factor in air just reflects the internal damping, that is  $Q_{int}=Q_{air}$ . When the NPLs are placed in a liquid environment, the damping has contributions from internal damping and liquid damping. In terms of quality factors, the total damping  $Q_{tot}$  in the liquid is  $\frac{1}{Q_{tot}}=\frac{1}{Q_{liq}}+\frac{1}{Q_{int}}$ , where  $Q_{liq}$  denotes the damping effects from the liquid. Thus, by comparing air and liquid measurements for a given NPL, we can determine the quality factor for liquid damping  $Q_{liq}$ .

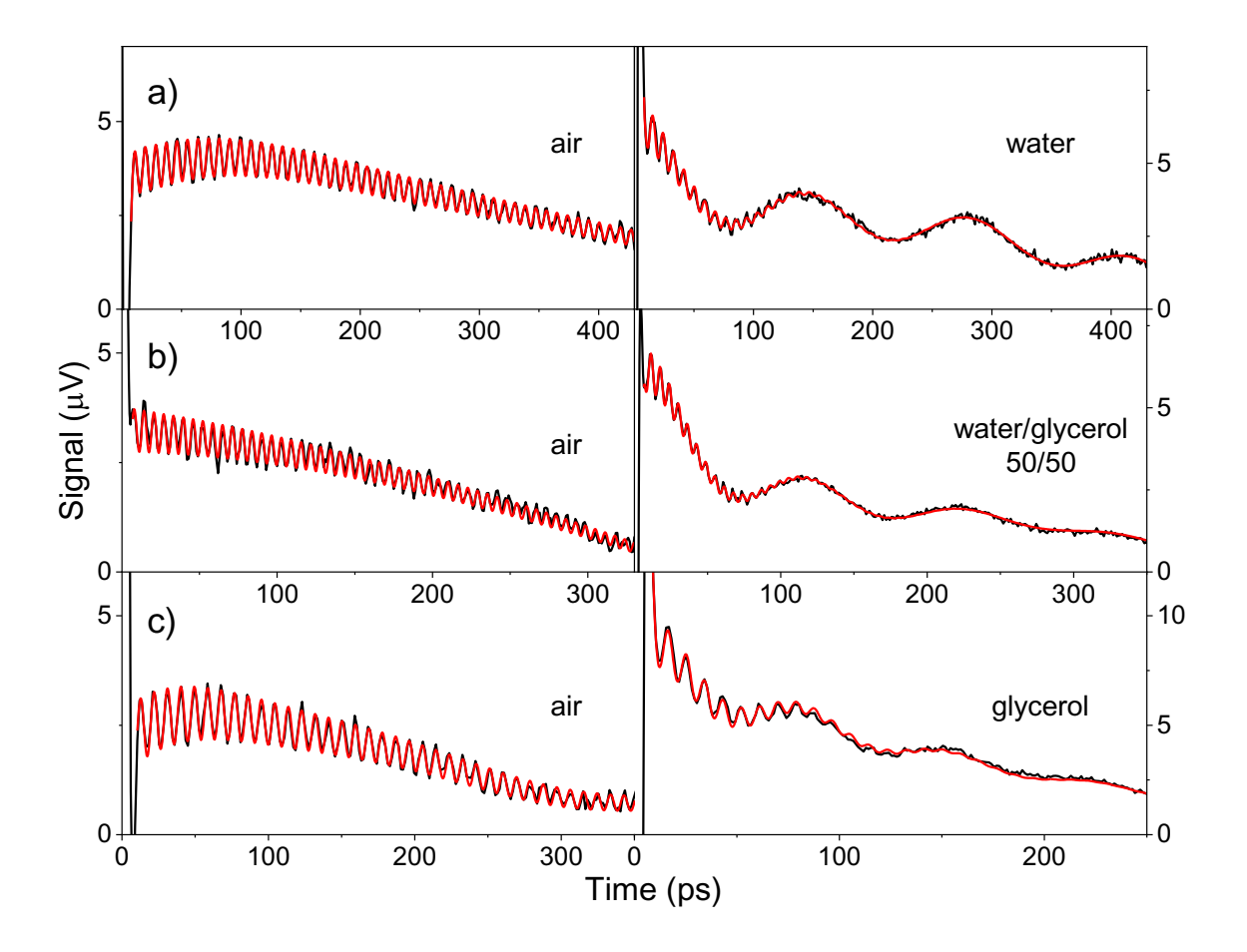


Figure 2. Transient absorption traces of single suspended Au NPLs in different environments: (a) air and water, (b) air and a mixture of 50% glycerol and 50% water by volume (corresponding to  $\chi_{gly}=0.56$  weight percent of glycerol in glycerol-water mixtures), (c) air and glycerol. The red lines are fits to the experimental data using equation 1. Fit parameters for the acoustic modes are: (a)  $f_{air}=112.88\pm0.03$  GHz,  $Q_{air}=140\pm11$ ,  $f_{water}=114.2\pm0.3$  GHz,  $Q_{water}=19\pm2$ ; (b)  $f_{air}=158.33\pm0.08$  GHz,  $Q_{air}=114\pm12$ ,  $f_{\chi=0.56}=159.8\pm0.3$  GHz,  $Q_{\chi=0.56}=18\pm2$ ; and (c)  $f_{air}=109.03\pm0.03$  GHz,  $Q_{air}=96\pm9$ ,  $f_{glycerol}=112.1\pm0.3$  GHz,  $Q_{glycerol}=15\pm2$ . The traces in the right panels also show Brillouin oscillations with (a)  $f_{water}^B=7.32\pm0.05$  GHz,  $Q_{water}^B=13\pm2$ ; (b)  $f_{\chi=0.56}^B=9.36\pm0.05$  GHz,  $Q_{\chi=0.56}^B=4\pm1$ ; and (c)  $f_{glycerol}^B=13.97\pm0.09$  GHz,  $Q_{glycerol}^B=5\pm1$ .

Figure 2 shows the representative transient absorption traces for single Au NPLs in different environments. Fitting the data using Equation 1 gives the vibrational frequencies and quality factors for the Au NPLs in the corresponding media. The fitting parameters are listed in the figure caption. There are several important points to note about the breathing mode vibrations. First, there is a slight increase of the vibrational frequency of the Au NPLs in liquids compared to the corresponding NPLs in air. The results are consistent with the corresponding FFT spectra shown in Figure S3. We notice that the fitting errors of the vibrational frequencies for Au NPLs in liquids are much larger (~0.3%) than that for the NPLs in air (~0.03%). The aggregated system errors for the vibrational frequency of Au NPLs in liquids are shown in Figure S2, and have a value of ~0.54% which is four times larger than that for Au NPLs in air (~0.13%). However, the increase in frequency observed when the NPLs are placed in liquid is larger than the experimental errors – see Figure S4. This effect is most obvious for the NPLs vibrating in glycerol. We believe the increase of the vibrational frequency in the liquid is due to a ligand releasing effect that is caused by the laser beam heating.<sup>27</sup>

The second effect from adding liquid to the samples is that there is a dramatic decrease in the vibrational quality factors. By correlating the lifetime measurements for the same single Au NPL in air and liquid, the damping of the liquid  $Q_{liq}$  is obtained. Figure 3(a) shows a statistical analysis of the quality factor for liquid damping for NPLs in water, a glycerol/water mixture with glycerol weight percent of  $\chi_{gly}=0.56$ , and glycerol. The raw data for the air and liquid experiments is presented in Figure S5. The average quality factors for liquid damping determined from this data are  $Q_{water}=24.6\pm3.9$ ,  $Q_{\chi=0.56}=21.2\pm2.3$  and  $Q_{glycerol}=16.1\pm2.4$  (errors are standard deviations). This data, and the quality factors for other glycerol/water mixtures are

collected in Table 1 below. Understanding the decrease of vibrational quality factors when liquid is added, and the associated fluid damping mechanism is the major goal of this study.

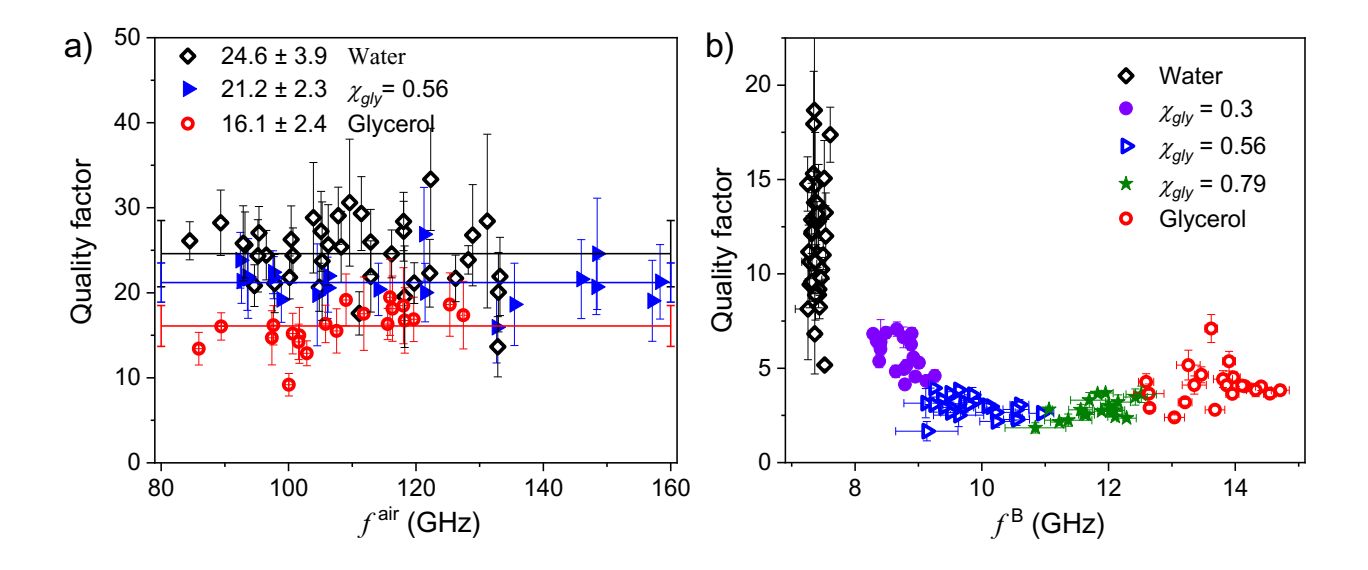


Figure 3. Confined acoustic vibrations of single Au NPLs and the propagating sound waves in different environments (multiple Au NPLs were tested for statistical analysis, see Table 1). (a) Quality factors for damping of the fundamental breathing mode by water, a glycerol/water mixture with  $\chi_{gly}=0.56$  and glycerol. The average quality factors are  $Q_{water}=24.6\pm3.9$ ,  $Q_{\chi=0.56}=21.2\pm2.3$  and  $Q_{glycerol}=16.1\pm2.4$ , respectively (errors are standard deviations). (b) Measured Brillouin oscillation frequencies and quality factors in water, and glycerol/water mixtures with varied glycerol weight percent. The average frequencies and quality factors are listed in Table 1.

In addition to the fundamental breathing mode of Au NPLs, there is another oscillating signal in Figure 2 for the Au NPLs in a liquid medium. This signal is assigned to Brillouin

oscillations that arises from the interaction of light with propagating sound waves in the liquid.<sup>28</sup> Au NPLs are excellent opto-acoustic transducers for generating propagating sound waves in liquids.<sup>28</sup> The frequency of the Brillouin oscillations  $f^B$  depends on the refractive index  $(n_f)$  and speed of sound  $(c_f)$  of the fluid:  $f^B = 2c_f n_f \cos \phi/\lambda_{pr}$ , where  $\phi$  is the angle of incidence of the probe beam and  $\lambda_{pr}$  is the probe beam wavelength. Under normal incidence, the frequency expression reduces to  $f^B = 2c_f n_f/\lambda_{pr}$ . Figure 3(b) shows a scatter plot of the quality factor versus frequency for the Brillouin oscillations measured for different NPLs in different liquids. The average Brillouin oscillation frequencies and quality factors from the data in Figure 3(b) are listed in Table 1. The errors are standard deviations. Using a refractive index n = 1.33 of water and  $f^B_{water} = 7.4 \pm 0.1$  GHz at 530 nm, we calculate a speed of sound of  $c_{water} = 1474 \pm 3$  m/s, which is consistent with previous results.<sup>16, 28</sup> However, the calculated speed of sound in glycerol is  $c_{glycerol} = 2470 \pm 47$  m/s, which is considerably larger than the literature value of 1930 m/s.<sup>32, 33</sup> Note that the errors for the Brillouin frequency in glycerol and glycerol/water mixture are much larger than that in water.

Table 1. Number of measurements N, Quality factors for the breathing modes of the nanoplates in air and quality factors for liquid damping Q, Brillouin oscillation frequencies  $f^B$  probed at 530 nm and quality factors  $Q^B$ , calculated speed of sound in the liquid  $c_B$ , and the liquid relaxation times derived from the vibrational quality factors ( $\lambda_{liq}$ ) and Brillouin oscillation ( $\lambda^B$ ) experiments. Errors are standard deviations for Q,  $f^B$  and  $Q^B$ , and 95% confidence limits for the  $c_B$ ,  $\lambda_{liq}$  and  $\lambda^B$ .

	N	Q	$f^{B}$ (GHz)	$Q^B$	$c_B$ (m/s)	$\lambda_{liq}$ (ps)	$\lambda^{B}$ (ps)
water	38	$24.6 \pm 3.9$	$7.4 \pm 0.1$	12 ± 4	1474 ± 3	1.1 +0.9/-0.5	
$\chi_{gly} = 0.56$	20	21.2 ± 2.3	$10.0 \pm 0.8$	$3.0 \pm 0.5$	1880 ± 67	14 +6/-4	8 ± 6
glycerol	21	16.1 ± 2.4	$13.7 \pm 0.6$	4 ± 1	2470 ± 47	700 +300/-170	700 ± 50

## Theoretical analysis

To analyze the results we follow the theoretical analysis of nanoparticle vibrations in liquids by Galstyan  $et~al.^{16}$  A detailed description of the derivation for the breathing mode vibrations of NPLs is presented in the Supporting Information. In this analysis the Navier equation is used to describe the displacement in the NPL, and the motion of the liquid is described by the Navier-Stokes equation. Assuming harmonic time dependence, a standing wave for the displacement in the plate, and outgoing waves for the fluid  $(e^{\pm ik_fz}e^{-i\omega t})$  where  $k_f$  is the wavevector for the fluid), matching the stress and velocity for the fluid and solid at the NPL surfaces yields the following eigenvalue equation for the frequency:

$$2ic_s\rho_s\sqrt{\rho_f(c_f^2\rho_f - i\omega\beta)} + \left(c_s^2\rho_s^2 + \rho_f(c_f^2\rho_f - i\omega\beta)\right)\tan\left(\frac{\hbar\omega}{c_s}\right) = 0$$
 (2)

where h is the thickness of the NPL,  $c_s$  and  $c_f$  are the speed of longitudinal sound waves in the solid and fluid, and  $\rho_s$  and  $\rho_f$  are the density of the solid and fluid, respectively.  $\beta = \kappa + 4\eta/3$ , where  $\eta$  is the shear viscosity and  $\kappa$  is the bulk viscosity of the fluid. Note that the wavevector in the fluid is given by  $k_f = \omega/\left(c_f\sqrt{1-i\omega\beta/c_f^2\rho_f}\right)$ . Equation (2) can be solved numerically to determine  $\omega$ . The frequency and quality factor of the breathing mode vibrations are then obtained by  $f = Re[\omega]/2\pi$  and  $Q = Re[\omega]/2Im[\omega]$ . For Au NPLs vibrating in an inviscid fluid medium ( $\kappa = \eta = 0$ ,  $\beta = 0$ ), where the damping is simply due to generation of sound waves in the fluid, Equation (2) reduces to:

$$2ic_s\rho_s c_f \rho_f + \left(c_s^2 \rho_s^2 + c_f^2 \rho_f^2\right) \tan\left(\frac{h \,\omega}{c_s}\right) = 0 \tag{3}$$

which is equivalent to the result of Fedou *et al.*<sup>37</sup> for the damping of NPLs in solid environments. Fluid viscoelasticity can be included in this analysis by scaling the fluid viscosities by

$$\kappa \to \kappa/(1 - i\lambda\omega)$$
 and  $\eta \to \eta/(1 - i\lambda\omega)$  (4)

where  $\lambda$  is the relaxation time in the liquid (here we assume that the relaxation time is the same for the shear and bulk viscosities). When the relaxation time for the fluid  $\lambda$  is comparable with the vibrational time scale  $1/\omega$ , the fluid has a large Deborah number and viscoelastic effects become significant. In contrast, the fluid turns into a Newtonian viscous fluid if the relaxation time is  $\lambda = 0$ .

Figures 4(a) and 4(b) show calculations of the breathing mode quality factors *versus* frequency for Au NPLs in water and glycerol. The dash lines are the quality factors calculated for an inviscid liquid (Equation (3)) where the shear and bulk viscosities are set to zero. The solid green lines are calculations for a viscous fluid ( $\lambda = 0$ ), and the solid blue lines are the calculations

for a viscoelastic fluid. The parameters used in these calculations were taken from Ref. [16], and the frequency was varied by changing the NPL thickness. The markers correspond to the experimental results, with the error bars indicating the standard deviations in 4(a), 4(b) and 4(c), and 95% confidence limits in 4(d). The results show that for water both the viscous and viscoelastic models are in reasonable agreement with the experimental data, whereas, for glycerol only the viscoelastic model gives a correct description of the damping.

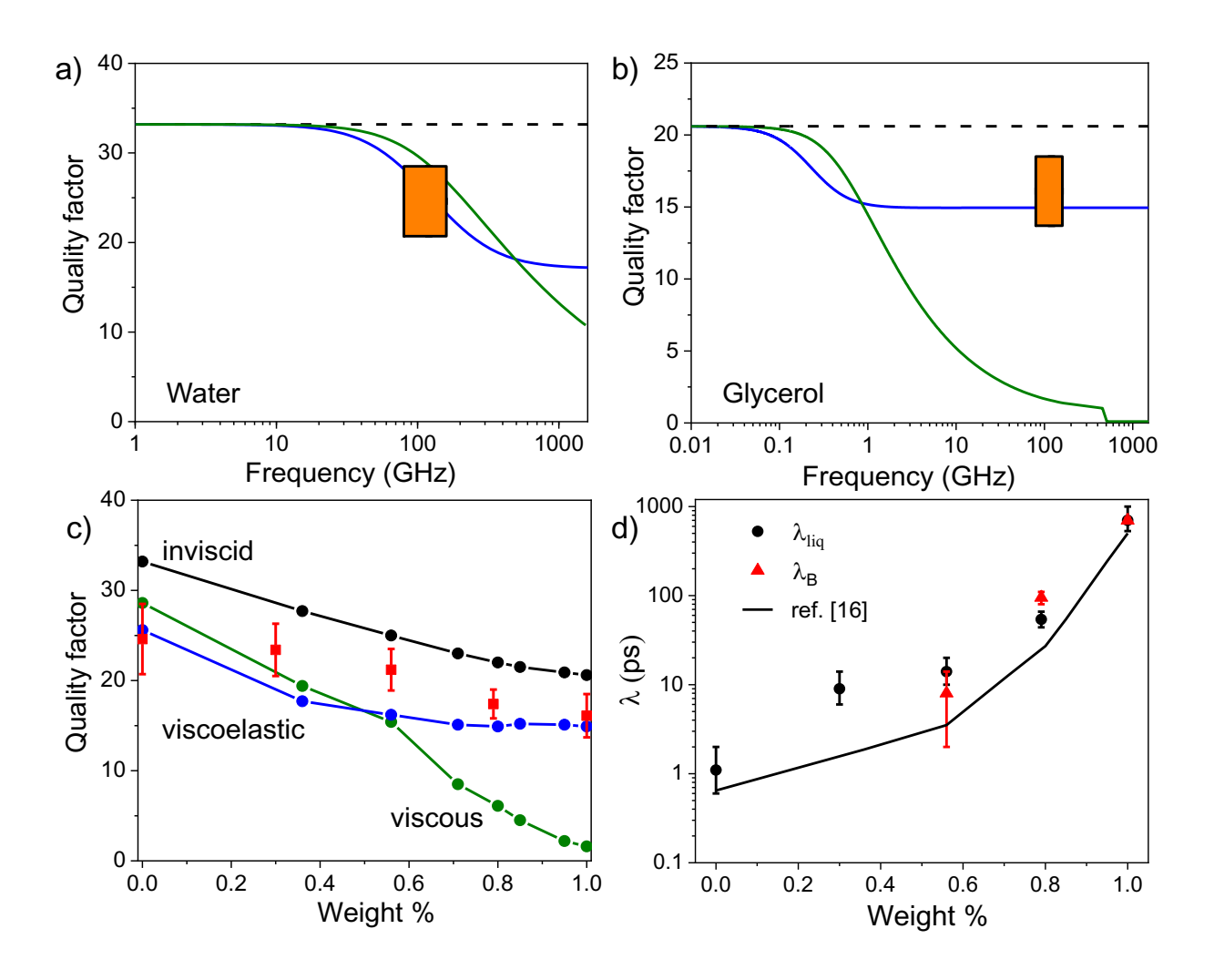


Figure 4. Calculated quality factors *versus* frequency for Au NPLs in (a) water and (b) glycerol. The dashed black lines correspond to an inviscid liquid, and the solid green and blue lines are

calculations for a viscous fluid and a viscoelastic fluid, respectively. The markers show the experimental results, where the error bars are standard deviations. (c) Plot of quality factor *versus* weight percent glycerol in glycerol-water mixtures. Lines and symbols have the same meaning as in panels (a) and (b). Calculations were performed using the liquid parameters given in Ref. [16]. (d) Calculated molecular relaxation times  $\lambda_{liq}$  and  $\lambda^B$ , based on the damping of the acoustic vibrations and sound wave velocities, respectively, errors are 95% confidence limits. The line shows the relaxation times given in Ref. [16].

Figure 4(c) shows a comparison of the measured and calculated quality factors for liquids with different weight percentages of glycerol. The calculations were performed for NPLs with a vibrational frequency of 120 GHz (the average frequency for the experimental samples). The markers are the experimental measurements. This plot shows that the viscoelastic model gives the best description of the fluid damping over the entire water-glycerol composition range, indicating that fluid viscoelastic effects are important for this system. In our previous studies of the breathing modes of Au nanowires, the effects of fluid viscoelasticity were hidden by the inviscid response of the fluid. That is, the experimental measurements were not accurate enough to differentiate between the inviscid and viscoelastic models of the fluid. 15, 20 The higher frequencies and quality factors of the Au NPLs in the present experiments provide a much better system for investigating these subtle effects. Note that the experimental measurements can also be used to estimate the relaxation times for the different liquids. 19 In these calculations the speed of sound and viscosity of the liquid were held constant, and the relaxation time was adjusted to match the experiments. The results are given in Table 1 and Figure 4(d). The relaxation times derived from our measurements are similar in magnitude, but consistently larger than the literature values.

The last point examined in this paper is the difference between the speeds of sound measured from the Brillouin oscillations and the literature values. Table 1 shows the calculated values from our transient absorption experiments. We find sound velocities varying from 1474  $\pm$ 3 m/s to  $2470 \pm 47 m/s$  for the glycerol/water mixtures from the Brillouin oscillation experiments. The value for water is within experimental error of the literature value (1510 m/s), but the value for glycerol is 28% higher that the literature value (1930 m/s). To understand this effect we note that viscosity modifies the wavevector in the fluid by  $k_f =$  $\omega/(c_f\sqrt{1-i\omega\beta/c_f^2\rho_f})$ . Thus, the speed of sound measured in the Brillouin oscillation experiments is modified by a factor of  $\sqrt{1-i2\pi f_B\beta/c_f^2\rho_f}$ . Using the viscoelastic model for the liquid ( $\beta \to \beta/(1-i\lambda 2\pi f_B)$ ) and values for  $\beta$ ,  $c_f$  and  $\rho_f$  from Ref. [16] predicts a 38% increase in the speed of sound for glycerol, which is consistent with the experimental observations. The Brillouin oscillation frequencies can also be used to estimate the liquid relaxation times, as was done above for the vibrational damping measurements. The values from this analysis are included in Table 1 and Figure 4(d), and are in reasonable agreements with the relaxation times obtained from the breathing mode experiments. Note that the relaxation times for water and the  $\chi_{gly}=0.3$ glycerol/water mixture can't be accurately determined in the Brillouin oscillation measurements. Recently, Brillouin spectroscopy was used to measure the relaxation times in biopolymer hydrogels for the characterization of biomechanical properties.<sup>48</sup> The measurement is limited to relatively low frequencies, which are mainly determine by the wavelength of the probe laser. In the current work, we realized that the high frequency acoustic vibrations provide better sensitivity over the Brillouin oscillations for determining the molecular relaxation times, especially for water which is the most biological relevant fluid. Thus, we anticipate an application of high frequency acoustic vibrations in biomechanics using the time-domain transient absorption spectroscopy.

## **CONCLUSIONS**

We synthesized Au NPLs with thickness of ~10 nm and large in-plane areas. The acoustic vibrations of single Au NPLs were characterized by time-resolved pump-probe microscopy experiments. The high quality factor mechanical vibrations of Au NPLs were used to probe fluidnanostructure interaction. Simple liquids, including water, glycerol and glycerol/water mixtures were analyzed. The measured quality factors were found to be significantly different to the values expected for an inviscid liquid (damping controlled by simple radiation of sound waves into the liquid). The experiments were modelled using a continuum mechanics theory for the damping of NPLs in liquids. Comparison between the calculations and experiments show that viscoelastic effects in the fluid are important for this system. The accurate fluid damping measurements in this work were also used to estimate the molecular relaxation times of the fluid (see Table 1 above). It further shows that the high frequency acoustic vibrations provide better sensitivity in probing fluid viscous and viscoelastic properties than Brillouin waves. The results from this study demonstrate that transient absorption microscopy measurements are a powerful method to probe the viscoelastic response of fluids. In particular, it may be possible to exploit the inherent sub-micron spatial resolution of these experiments to obtain fluid mechanics information about cellular systems.

#### **EXPERIMENTAL METHODS**

**Materials.** HAuCl<sub>4</sub>·3H<sub>2</sub>0, 1-pentanol, Glycerol, CTAB and PVP (Mn = 40,000) were purchased from Sigma-Aldrich. Ethanol was purchased from Sinopharm Chemical Reagent Co. Ultrapure

water was used throughout the experiments. Holey silicon nitride films with pore size of  $\sim 5 \mu m$  and thickness of  $\sim 200$  nm were purchased from Ted Pella Inc. (catalog no. 21536).

Au nanoplates synthesis. The Au NPLs were synthesized using a modified method. 40, 41 Briefly, a mixture of HAuCl<sub>4</sub>·3H<sub>2</sub>0 1-pentanol solution (10 mL, 0.02 mm) with CTAB water solution (0.5 mL, 0.2 M) was heated to 110 °C until fully transparent. PVP (Mn= 40,000, 74 mg) dissolved in 1-pentanol (3 mL) was then added drop by drop. The final solution was kept at 110 °C for 10 hours to facilitate the growth of Au NPLs. The yellow product was collected and washed with ethanol three times by centrifugation to remove excessive surfactants before drop-casting on the holey silicon nitride film. After Au NPLs deposited on silicon nitride films, they were immersed in water at 30 °C for 12 hours to trying to minimize the surfactant on Au NPLs surfaces. The sample is air dried and ready for vibrational measurements. Note that only the Au NPLs suspended over the pores of silicon nitride films are investigated for the study of liquid effects. Only thin Au NPLs with acoustic vibration frequencies above ~100 GHz were selected for the study of liquid damping effect. The Au NPLs synthesized in the current studies have {111} surfaces with edge lengths of ~10-20 μm.

Femtosecond Transient Absorption Microscopy. The setup for transient absorption microscopy has been described earlier. A Coherent Mira 900 Ti:sapphire oscillator combined with Coherent Mira optical parametric oscillator (OPO) laser system is used for the pump-probe measurements. The 800 nm pump beam from the Ti:sapphire oscillator was modulated at 1 MHz by an acousto-optic modulator (IntraAction AOM-402AF3), triggered by the internal function generator of a lock-in amplifier (Stanford Research Systems SR844). The probe beam from the OPO was tuned to 530 nm and overlapped with the pump beam and focused at a single Au NPL with an Olympus  $100 \times 1.4$  NA microscope objective. Note that the polarizations of the pump and probe beams

were made linear and circular before the objective lens, respectively. The delay time between the pump and probe beams was controlled by a Thorlabs DDS600 linear translation stage. The measurements were performed in reflection mode by monitoring the reflected probe beam intensity with an avalanche photodiode (APD, Hamamatsu C12702-11) and the lock-in amplifier at a time constant of 30 ms. Typical powers were 3 mW for the pump and 100 μW for the probe. Under these conditions, the signal was stable and no melting or reshaping of the Au NPLs was observed. The confined acoustic vibrations of Au NPLs can be excited due to the absorption of the pump power. These acoustic vibrations cause periodic changes of the thickness of the nanoplate and thus of the absorption of the probe, and consequently are detected by monitoring the probe beam intensity.<sup>6, 8, 49</sup> A signal due to the propagating acoustic waves in the liquids, known as Brillouin oscillations, is also detected. This signal arises from interference between the reflected probe beams from the NPL surface and acoustic waves generated in the liquid by rapid laser induced heating of the sample.<sup>28, 31, 50</sup>

#### SUPPORTING INFORMATION

The Supporting Information is available free of charge at ACS website.

Large area SEM image, characterization of system errors, FFT spectra of the acoustic vibrations in Figure 2, vibration frequency changes in different environments, the measured vibrational quality factors of Au NPLs in liquids, and detailed theoretical analysis of the breathing mode in a fluid.

Acknowledgements: The authors acknowledge the support of the National Natural Science

Foundation of China (Grant 11734012, 12074266, 12074267), the Science and Technology Project

of Guangdong (Grant 2020B010190001) and the Innovation Commission of Shenzhen (Grant

JCYJ20190808154613434). GVH acknowledges the support of the National Science Foundation

through Award CHE-2002300.

**Corresponding Authors:** 

Email: kyu@szu.edu.cn

Email: ghartlan@nd.edu

Email: gpwang@szu.edu.cn

**ORCID:** 

Kuai Yu: 0000-0001-6138-0367

Gregory V. Hartland: 0000-0002-8650-6891

22

#### References

- 1. Pelton, M.; Sader, J. E.; Burgin, J.; Liu, M.; Guyot-Sionnest, P.; Gosztola, D., Damping of Acoustic Vibrations in Gold Nanoparticles. *Nat. Nanotechnol.* **2009**, *4* (8), 492-5.
- 2. Xiang, D.; Wu, J.; Rottler, J.; Gordon, R., Threshold for Terahertz Resonance of Nanoparticles in Water. *Nano Lett.* **2016**, *16* (6), 3638-3641.
- 3. Muskens, O. L.; Del Fatti, N.; Vallée, F., Femtosecond Response of a Single Metal Nanoparticle. *Nano Lett.* **2006**, *6* (3), 552-556.
- 4. Maioli, P.; Stoll, T.; Sauceda, H. E.; Valencia, I.; Demessence, A.; Bertorelle, F.; Crut, A.; Vallee, F.; Garzon, I. L.; Cerullo, G.; Del Fatti, N., Mechanical Vibrations of Atomically Defined Metal Clusters: From Nano- to Molecular-Size Oscillators. *Nano Lett.* **2018**, *18* (11), 6842-6849.
- 5. Juvé, V.; Crut, A.; Maioli, P.; Pellarin, M.; Broyer, M.; Del Fatti, N.; Vallée, F., Probing Elasticity at the Nanoscale: Terahertz Acoustic Vibration of Small Metal Nanoparticles. *Nano Lett.* **2010,** *10* (5), 1853-1858.
- 6. Hu, M.; Wang, X.; Hartland, G. V.; Mulvaney, P.; Juste, J. P.; Sader, J. E., Vibrational Response of Nanorods to Ultrafast Laser Induced Heating: Theoretical and Experimental Analysis. *J. Am. Chem. Soc.* **2003**, *125* (48), 14925-14933.
- 7. Hartland, G. V., Optical Studies of Dynamics in Noble Metal Nanostructures. *Chem. Rev.* **2011,** *111* (6), 3858-3887.
- 8. van Dijk, M. A.; Lippitz, M.; Orrit, M., Detection of Acoustic Oscillations of Single Gold Nanospheres by Time-Resolved Interferometry. *Phys. Rev. Lett.* **2005**, *95* (26), 267406.
- 9. Gil-Santos, E.; Baker, C.; Nguyen, D. T.; Hease, W.; Gomez, C.; Lemaitre, A.; Ducci, S.; Leo, G.; Favero, I., High-Frequency Nano-Optomechanical Disk Resonators in Liquids. *Nat. Nanotechnol.* **2015**, *10* (9), 810-6.

- 10. Gil-Santos, E.; Ruz, J. J.; Malvar, O.; Favero, I.; Lemaitre, A.; Kosaka, P. M.; Garcia-Lopez, S.; Calleja, M.; Tamayo, J., Optomechanical Detection of Vibration Modes of a Single Bacterium. *Nat. Nanotechnol.* **2020**, *15* (6), 469-474.
- 11. Fernandes, D. B.; Spuch-Calvar, M.; Baida, H.; Tréguer-Delapierre, M.; Oberlé, J.; Langot, P.; Burgin, J., Acoustic Vibrations of Au Nano-Bipyramids and their Modification under Ag Deposition: a Perspective for the Development of Nanobalances. *ACS Nano* **2013**, *7* (9), 7630-7639.
- 12. Ruijgrok, P. V.; Zijlstra, P.; Tchebotareva, A. L.; Orrit, M., Damping of Acoustic Vibrations of Single Gold Nanoparticles Optically Trapped in Water. *Nano Lett.* **2012**, *12* (2), 1063-1069.
- 13. Yu, K.; Sader, J. E.; Zijlstra, P.; Hong, M.; Xu, Q.-H.; Orrit, M., Probing Silver Deposition on Single Gold Nanorods by Their Acoustic Vibrations. *Nano Lett.* **2014**, *14* (2), 915-922.
- 14. Pelton, M.; Chakraborty, D.; Malachosky, E.; Guyot-Sionnest, P.; Sader, J. E., Viscoelastic Flows in Simple Liquids Generated by Vibrating Nanostructures. *Phys. Rev. Lett.* **2013**, *111* (24), 244502.
- 15. Yu, K.; Major, T. A.; Chakraborty, D.; Devadas, M. S.; Sader, J. E.; Hartland, G. V., Compressible Viscoelastic Liquid Effects Generated by the Breathing Modes of Isolated Metal Nanowires. *Nano Lett.* **2015**, *15* (6), 3964-3970.
- 16. Galstyan, V.; Pak, O. S.; Stone, H. A., A Note on the Breathing Mode of an Elastic Sphere in Newtonian and Complex Fluids. *Phys. Fluids* **2015**, *27* (3), 032001.
- 17. Chakraborty, D.; Sader, J. E., Constitutive Models for Linear Compressible Viscoelastic Flows of Simple Liquids at Nanometer Length Scales. *Phys. Fluids* **2015**, *27* (5), 052002.

- 18. Marty, R.; Arbouet, A.; Girard, C.; Mlayah, A.; Paillard, V.; Lin, V. K.; Teo, S. L.; Tripathy, S., Damping of the Acoustic Vibrations of Individual Gold Nanoparticles. *Nano Lett.* **2011**, *11* (8), 3301-3306.
- 19. Chakraborty, D.; Hartland, G. V.; Pelton, M.; Sader, J. E., When Can the Elastic Properties of Simple Liquids Be Probed Using High-Frequency Nanoparticle Vibrations? *J. Phys. Chem. C* **2017**, *122* (25), 13347-13353.
- 20. Devkota, T.; Chakraborty, D.; Yu, K.; Beane, G.; Sader, J. E.; Hartland, G. V., On the Measurement of Relaxation Times of Acoustic Vibrations in Metal Nanowires. *Phys. Chem. Chem. Phys.* **2018**, *20* (26), 17687-17693.
- 21. Girard, A.; Gehan, H.; Crut, A.; Mermet, A.; Saviot, L.; Margueritat, J., Mechanical Coupling in Gold Nanoparticles Supermolecules Revealed by Plasmon-Enhanced Ultralow Frequency Raman Spectroscopy. *Nano Lett.* **2016**, *16* (6), 3843-3849.
- 22. Clark, J. N.; Beitra, L.; Xiong, G.; Higginbotham, A.; Fritz, D. M.; Lemke, H. T.; Zhu, D.; Chollet, M.; Williams, G. J.; Messerschmidt, M.; Abbey, B.; Harder, R. J.; Korsunsky, A. M.; Wark, J. S.; Robinson, I. K., Ultrafast Three-Dimensional Imaging of Lattice Dynamics in Individual Gold Nanocrystals. *Science* **2013**, *341* (6141), 56-59.
- 23. Crut, A.; Maioli, P.; Del Fatti, N.; Vallée, F., Acoustic Vibrations of Metal Nano-Objects: Time-Domain Investigations. *Phys. Rep.* **2015**, *549*, 1-43.
- 24. Beane, G.; Devkota, T.; Brown, B. S.; Hartland, G. V., Ultrafast Measurements of the Dynamics of Single Nanostructures: a Review. *Rep Prog Phys* **2019**, *82* (1), 016401.
- 25. Wang, J.; Yang, Y.; Wang, N.; Yu, K.; Hartland, G. V.; Wang, G. P., Long Lifetime and Coupling of Acoustic Vibrations of Gold Nanoplates on Unsupported Thin Films. *J. Phys. Chem. A* **2019**, *123* (47), 10339-10346.

- 26. Wang, J.; Yu, K.; Yang, Y.; Hartland, G. V.; Sader, J. E.; Wang, G. P., Strong Vibrational Coupling in Room Temperature Plasmonic Resonators. *Nat. Commun.* **2019**, *10* (1), 1527.
- 27. Devkota, T.; Yu, K.; Hartland, G. V., Mass loading effects in the acoustic vibrations of gold nanoplates. *Nanoscale* **2019**, *11* (35), 16208-16213.
- 28. Yu, K.; Devkota, T.; Beane, G.; Wang, G. P.; Hartland, G. V., Brillouin Oscillations from Single Au Nanoplate Opto-Acoustic Transducers. *ACS Nano* **2017**, *11* (8), 8064-8071.
- 29. Vitalyi, E. G.; Pascal, R., Advances in Applications of Time-Domain Brillouin Scattering for Nanoscale Imaging. *Appl. Phys. Rev.* **2018**, *5* (3), 031101.
- 30. Chaban, I.; Shin, H. D.; Klieber, C.; Busselez, R.; Gusev, V. E.; Nelson, K. A.; Pezeril, T., Time-Domain Brillouin Scattering for the Determination of Laser-Induced Temperature Gradients in Liquids. *Rev. Sci. Instrum.* **2017**, *88* (7), 074904.
- 31. Ruello, P.; Gusev, V. E., Physical Mechanisms of Coherent Acoustic Phonons Generation by Ultrafast Laser Action. *Ultrasonics* **2015**, *56*, 21-35.
- 32. Pezeril, T.; Klieber, C.; Andrieu, S.; Nelson, K. A., Optical Generation of Gigahertz-Frequency Shear Acoustic Waves in Liquid Glycerol. *Phys. Rev. Lett.* **2009**, *102* (10), 107402.
- 33. Klieber, C.; Hecksher, T.; Pezeril, T.; Torchinsky, D. H.; Dyre, J. C.; Nelson, K. A., Mechanical Spectra of Glass-Forming Liquids. II. Gigahertz-Frequency Longitudinal and Shear Acoustic Dynamics in Glycerol and DC704 Studied by Time-Domain Brillouin Scattering. *J. Chem. Phys.* **2013**, *138* (12), 12A544.
- 34. Klieber, C.; Pezeril, T.; Andrieu, S.; Nelson, K. A., Optical Generation and Detection of Gigahertz-Frequency Longitudinal and Shear Acoustic Waves in Liquids: Theory and Experiment. *J. Appl. Phys.* **2012**, *112* (1), 013502.

- 35. Girard, A.; Saviot, L.; Pedetti, S.; Tessier, M. D.; Margueritat, J.; Gehan, H.; Mahler, B.; Dubertret, B.; Mermet, A., The Mass Load Effect on the Resonant Acoustic Frequencies of Colloidal Semiconductor Nanoplatelets. *Nanoscale* **2016**, *8* (27), 13251-13256.
- 36. Malvar, O.; Ruz, J. J.; Kosaka, P. M.; Domínguez, C. M.; Gil-Santos, E.; Calleja, M.; Tamayo, J., Mass and Stiffness Spectrometry of Nanoparticles and Whole Intact Bacteria by Multimode Nanomechanical Resonators. *Nat. Commun.* **2016**, *7*, 13452.
- 37. Fedou, J.; Viarbitskaya, S.; Marty, R.; Sharma, J.; Paillard, V.; Dujardin, E.; Arbouet, A., From Patterned Optical Near-Fields to High Symmetry Acoustic Vibrations in Gold Crystalline Platelets. *Phys. Chem. Chem. Phys.* **2013**, *15* (12), 4205-4213.
- 38. Großmann, S.; Friedrich, D.; Karolak, M.; Kullock, R.; Krauss, E.; Emmerling, M.; Sangiovanni, G.; Hecht, B., Nonclassical Optical Properties of Mesoscopic Gold. *Phys. Rev. Lett.* **2019**, *122* (24), 246802.
- 39. Viarbitskaya, S.; Teulle, A.; Marty, R.; Sharma, J.; Girard, C.; Arbouet, A.; Dujardin, E., Tailoring and Imaging the Plasmonic Local Density of States in Crystalline Nanoprisms. *Nat. Mater.* **2013**, *12* (5), 426-432.
- 40. Wang, C.; Kan, C.; Zhu, J.; Zeng, X.; Wang, X.; Li, H.; Shi, D., Synthesis of High-Yield Gold Nanoplates: Fast Growth Assistant with Binary Surfactants. *J. Nanomater.* **2010**, *2010*, 969030.
- 41. Krauss, E.; Kullock, R.; Wu, X.; Geisler, P.; Lundt, N.; Kamp, M.; Hecht, B., Controlled Growth of High-Aspect-Ratio Single-Crystalline Gold Platelets. *Cryst. Growth Des.* **2018**, *18* (3), 1297-1302.
- 42. Zhai, Y.; DuChene, J. S.; Wang, Y.-C.; Qiu, J.; Johnston-Peck, A. C.; You, B.; Guo, W.; DiCiaccio, B.; Qian, K.; Zhao, E. W.; Ooi, F.; Hu, D.; Su, D.; Stach, E. A.; Zhu, Z.; Wei, W. D., Polyvinylpyrrolidone-Induced Anisotropic Growth of Gold Nanoprisms in Plasmon-Driven Synthesis. *Nat. Mater.* **2016**, *15*, 889.

- 43. Perner, M.; Gresillon, S.; März, J.; von Plessen, G.; Feldmann, J.; Porstendorfer, J.; Berg, K. J.; Berg, G., Observation of Hot-Electron Pressure in the Vibration Dynamics of Metal Nanoparticles. *Phys. Rev. Lett.* **2000**, *85* (4), 792-795.
- 44. Major, T. A.; Lo, S. S.; Yu, K.; Hartland, G. V., Time-Resolved Studies of the Acoustic Vibrational Modes of Metal and Semiconductor Nano-objects. *J. Phys. Chem. Lett.* **2014**, *5* (5), 866-874.
- 45. Besteiro, L. V.; Yu, P.; Wang, Z. M.; Holleitner, A. W.; Hartland, G. V.; Wiederrecht, G. P.; Govorov, A. O., The Fast and the Furious: Ultrafast Hot Electrons in Plasmonic Metastructures. Size and Structure Matter. *Nano Today* **2019**, *27*, 120-145.
- 46. Hartland, G. V., Statistical Analysis of Physical Chemistry Data: Errors Are Not Mistakes. *J Phys Chem A* **2020**, *124* (11), 2109-2112.
- 47. Saviot, L.; Netting, C. H.; Murray, D. B., Damping by Bulk and Shear Viscosity of Confined Acoustic Phonons for Nanostructures in Aqueous Solution. *J. Phys. Chem. B* **2007**, *111* (25), 7457-7461.
- 48. Bailey, M.; Alunni-Cardinali, M.; Correa, N.; Caponi, S.; Holsgrove, T.; Barr, H.; Stone, N.; Winlove, C. P.; Fioretto, D.; Palombo, F., Viscoelastic Properties of Biopolymer Hydrogels Determined by Brillouin Spectroscopy: A Probe of Tissue Micromechanics. *Sci. Adv.* **2020**, *6* (44), eabc1937.
- 49. Zijlstra, P.; Tchebotareva, A. L.; Chon, J. W. M.; Gu, M.; Orrit, M., Acoustic Oscillations and Elastic Moduli of Single Gold Nanorods. *Nano Lett.* **2008**, *8* (10), 3493-3497.
- 50. Thomsen, C.; Strait, J.; Vardeny, Z.; Maris, H. J.; Tauc, J.; Hauser, J. J., Coherent Phonon Generation and Detection by Picosecond Light Pulses. *Phys. Rev. Lett.* **1984**, *53* (10), 989-992.